Computation and theory

Electronic states of 3D aromatic molecules on Au(111) surfaces: adsorption of carboranethiol

Takuto Aoki[1], Yuta Nakahama[1], Tadao Ikeda[1], Masako Shindo[2], Masanobu Uchiyama[3], and Ken-ichi Shudo[1,3,*]

[1] *Department of Physics, Yokohama National University, Hodogaya-ku, Yokohama 240-8501, Japan*
[2] *Osaka Institute of Technology, Asahi-ku, Osaka 535-8585, Japan*
[3] *Cluster of Pioneering Research (CPR), Advanced Elements Chemistry Laboratory, RIKEN, Wako-shi, Saitama 351-0198, Japan*

ABSTRACT

To clarify the effect of covalent surface adsorption on the geometric and electronic structure of carboranes, *p*-carboranethiol (*p*CT) was deposited on clean Au(111) surfaces under vacuum and the resulting systems were probed by scanning tunneling microscopy, scanning tunneling spectroscopy and ultraviolet photoelectron spectroscopy. The spectral features observed at different *p*CT coverage levels revealed the emergence of new electronic states near the surface, which were analyzed using ab initio calculations. The resulting computational and experimental data are used to explain the contributions of these states to bonding between the substrate and adsorbate, resonance with metallic substrate states and substrate-mediated intermolecular interactions.

Introduction

Adsorbed organic molecules, particularly aromatic compounds, are used to tune the surface functionality of solid materials such as semiconductors and metals in many fields, including molecular electronics, gas capture devices and chemical sensors [1]. Since the discovery of fullerenes, carbon-based molecules with cage and honeycomb structures have attracted great interest from researchers despite their limited chemical reactivity [2]. More recently, the very stable icosahedral molecule carborane (1,12-$C_2B_{10}H_{12}$; see Fig. 1a) and its derivatives have emerged as new frameworks for three-dimensional molecular chemistry and superacidity [3]. Their

responses to radiation have been studied [4–7], and they have been shown to act as Mott insulators with dielectric correlations [8–10]. In addition, their strong electric dipoles have been exploited in ionic flow control systems and gas sensors [10–13]. In these applications, carborane derivatives are typically used as surface adsorbates or thin films.

It was recently shown that carboranes can serve as unique adsorbates to prepare next generation surface-functionalized materials. These functionalizations rely on the facile chemical derivatization of carboranes [14, 15], which is much more straightforward than the chemical modification of fullerenes. Carborane derivatives form robust thin films that retain stability at high temperatures [16] and exhibit
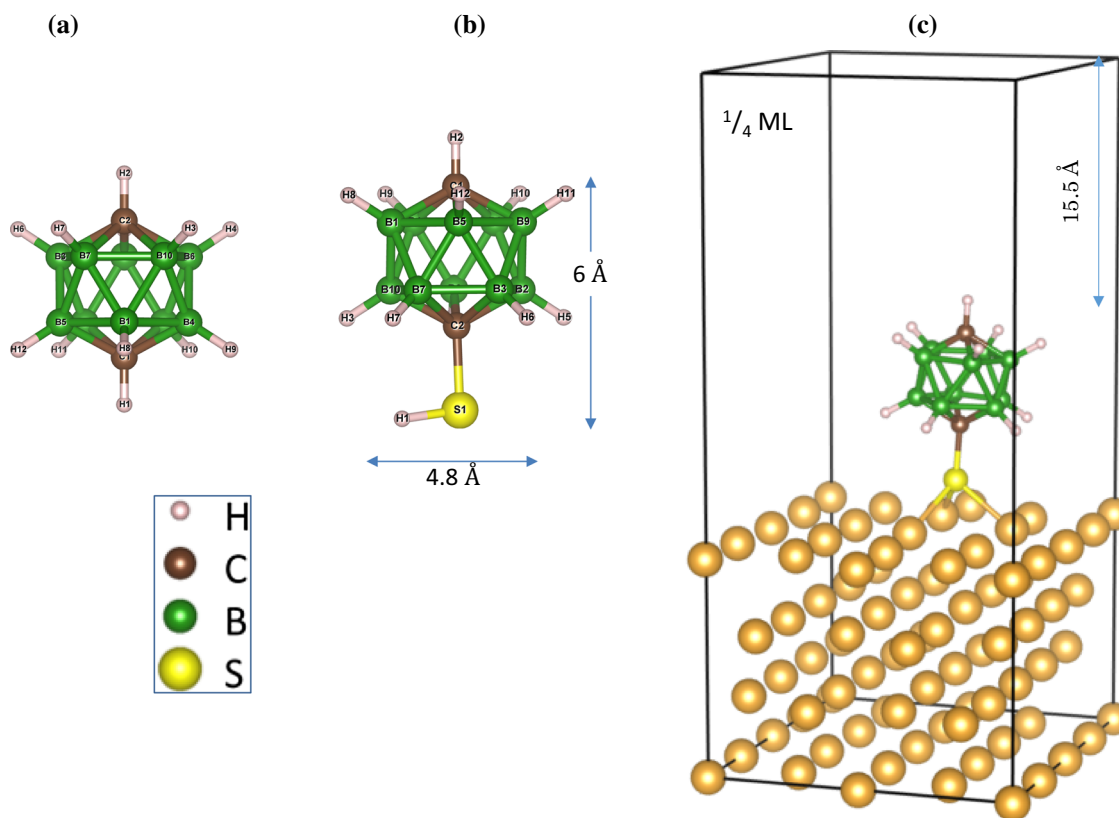

Address correspondence to E-mail: ken1@ynu.ac.jp

Springer

Figure 1 Structures of **a** *p*-carborane and **b** *p*CT molecules. **c** Structure of a *p*CT-adsorbed Au(111) surface at ∼ 1/4 ML coverage. All images show structures obtained after geometry optimization.

good air stability [17] despite their chemical reactivity. Importantly, *p*-carborane has little effect on the chemistry of functional groups bound to its carbon centers [18], making it a common benchmark species for surface modification. Organic thiols adsorb readily to metal surfaces [19], enabling a variety of surface functionalizations and the formation of homogeneous self-assembled monolayers (SAMs) with regular structures [17, 20, 21]. The adsorption of thiols on metal surfaces typically occurs with reductive elimination of hydrogen [22]:

$$R-SH + Au\,(111) \rightarrow R-S-Au\,(111) + \tfrac{1}{2}H_2 \qquad (1)$$

p-carboranethiol (1-HS-1,12-C$_2$B$_{10}$H$_{11}$; see Fig. 1b), and its derivatives are known to adsorb on metal surfaces in this way [17].

The positions of carboranes' electronic states relative to the Fermi level (E_F) when adsorbed on metals [23] can depend on their chemical environment and local adsorption structures, suggesting that it may be possible to tune their electronic properties to suit specific applications. Studies on the electronic states of carboranes physiadsorbed on a gold surface or

chemisorbed via an alkanethiol moiety have shown that the electronic states of the carborane shells closely resemble those of the isolated molecules: The gap between the occupied and empty states of the B–C shell was estimated to be very wide (8–11 eV) [23, 24]. Additionally, photoemission studies on carboranes physisorbed on metals [7–9] revealed a weak but clear correlation: The energies of unoccupied states tended to increase with the thickness of the film. However, it is not clear how a carborane's π-electrons interact with the metal when the B–C sphere is close to the metal surface. Also, unknown is the structure of the systems formed by adsorption when metal surfaces are exposed to carboranethiols out of solution. We therefore investigated the structure and electronic states of *p*-carboranethiol (*p*CT) directly adsorbed to a gold surface using scanning tunneling microscopy/spectroscopy (STM/STS) and ultraviolet photoemission spectroscopy (UPS). The obtained spectra were interpreted based on densities of state calculated from first principles and were related to the observed structures of the adsorbed species.

Methods

Experimental

A previously reported procedure (see Fig. 2) [25] was used to synthesize *p*CT. Briefly, 20 mL of a 0.05 M solution of carborane in hexane was poured into a suspension of NaNH$_2$ at room temperature prepared by adding sodium (2.3 g) to 200 mL of liquid ammonia containing 0.2 g of Fe(NO$_3$)$_3$ as a catalyst. Powdered S$_8$ (1.6 g) was then added to this suspension, and the resulting mixture was stirred for 1 h. After the elimination of ammonia and hexane in vacuum, ethanol and water were added. Unreacted carborane and other by-products were removed by extraction with hexane, and the desired product was obtained by repeated recrystallization from aqueous KHCO$_3$ to remove unwanted by-products such as the dithiol. Finally, we obtained *p*CT as a white crystalline powder whose NMR spectra matched those reported previously [25]. Note that *para* (1,12-) CT is the least acidic of the carboranethiol isomers; its reported pK_a is 5.9, compared to 5.3 and 3.3 for the *meta* (1,7-) and *ortho* (1,2-) isomers, respectively.

The gold films used as substrates were deposited ex situ (typical thickness: 600 Å) on mica using a DC sputter coater (JEOL, JFC-1500). Clean Au(111) surfaces were obtained by repeated Ar-ion sputtering at 600 eV and heating to 540 °C under ultrahigh vacuum (UHV) at 2×10^{-8} Pa. On the clean Au surface kept at room temperature, *p*CT was dosed from crystalline powder in a sealed test tube that was gently heated (to approximately human body temperature) through a precise leak valve attached to the UHV chamber. In this article, the gas exposure at the surface is expressed in units of Langmuirs (L), where $1 \text{ L} = 1.3 \times 10^{-4}$ Pa s.

Surface observations were performed by scanning tunneling microscopy/spectroscopy (STM/STS) using a JEOL microscope (JSTM-4500 XT) equipped with W tips produced by electrolytic polishing. All measurements were performed with the sample at room temperature in a UHV chamber. Prior to each experiment, the cleanliness of the Au(111) surface was confirmed by observing its herring-bone structure by STM [26, 27] and by using STS to confirm the presence of a weak peak indicative of a Shockley-type surface state at approximately 0.4 eV below E_F [28, 29].

The samples' electronic states were also characterized by ultraviolet photoemission spectroscopy (UPS). Samples for this purpose were prepared in a UHV chamber as described above and then irradiated with UV light from a homemade He discharger (He I, 21.2 eV) at 45° to the surface normal. The energy of the photoelectrons emitted in the direction normal to the surface was measured with a hemispherical analyzer (Thermo VG, CLAM-II).

Calculations

Theoretical calculations were performed to help interpret the experimental data. The geometry of the isolated *p*CT molecule was initially optimized using Gaussian 09 [30]. Its electronic states were computed by performing density functional theory calculations using the B3LYP hybrid correlation functional with the 6-31g* basis set. The energy distribution curves generated from the electronic eigenvalues of the optimized structures are referred to as densities of states (DOS) hereafter. The DOS plot for the isolated molecule was generated by smearing its eigenvalues using a Gaussian function having a width of ∼ 0.3 eV, after shifting so as to place E_F between the HOMO and LUMO.

To study the electronic state of the adsorbed system, we initially considered the *p*-carboranethiolate (the product in Eq. 1). The adsorbed structure and electronic spectra of *p*CT on Au(111) were obtained using the Vienna Ab initio Simulation Package (VASP) [31]. A *p*-carboranethiolate radical was placed on a four-layer Au slab in a 4 × 4 supercell. The vacuum layer depth was ∼ 15.5 Å (see Fig. 1c). The Perdew–Becke–Ernzerhof (PBE) potentials for the

Figure 2 Synthesis of *p*CT from *p*-carborane.

p-carborane
(purchased)

Na
liq. NH$_3$
Fe(NO$_3$)$_3$·9H$_2$O

S$_8$

*p*CT + byproduct
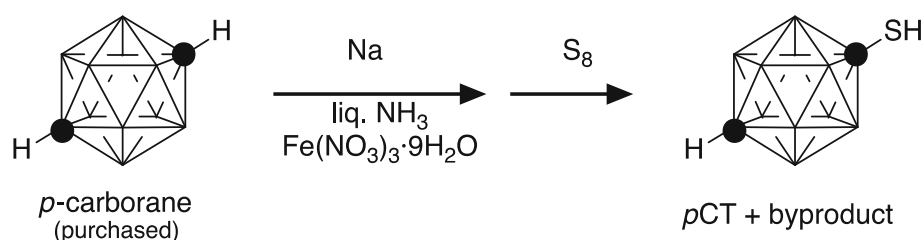
involved elements were used with a projector-augmented wave (PAW) functional. The cut-off energy and wavevector mesh were 400 eV and $4 \times 4 \times 1$, respectively. The dehydrogenated *p*-carboranethiolate radical (whose geometry was optimized using Gaussian 09) was placed on the metal substrate, and then the whole system was optimized using VASP.

Results

Adsorbed structure (STM/STS)

A clean Au(111) surface was exposed to a very low level of gaseous *p*CT (~ 0.01 L) to induce partial surface coverage. As shown in Fig. 3a, STM images acquired after *p*CT adsorption revealed the formation of cloudy protrusions, which were identified as

adsorbed *p*CT units. While some adsorbed molecules were present on the terrace and steps of the Au(111) surface, the terrace's characteristic herring-bone stripes remained clearly visible. The adsorbed molecules tended to aggregate into clusters. As the *p*CT exposure increased, the number and density of clusters increased. At an exposure of ~ 1 L, *p*CT clusters of varying size covered the whole Au surface; no flat terrace could be seen, and it was difficult to control or identify the size of the clusters.

Figure 3b presents STS spectra acquired at two points on the *p*CT-exposed Au(111) surface shown in Fig. 3a: one with no adsorbed *p*CT (point A) and one with an adsorbed *p*CT cluster (point B). The d*I*/d*V* signal of the cluster peaks was much stronger than that for the peaks of the intact gold terrace (point A). Moreover, the cluster spectrum has some oscillatory peaks not seen in the spectrum of the terrace.
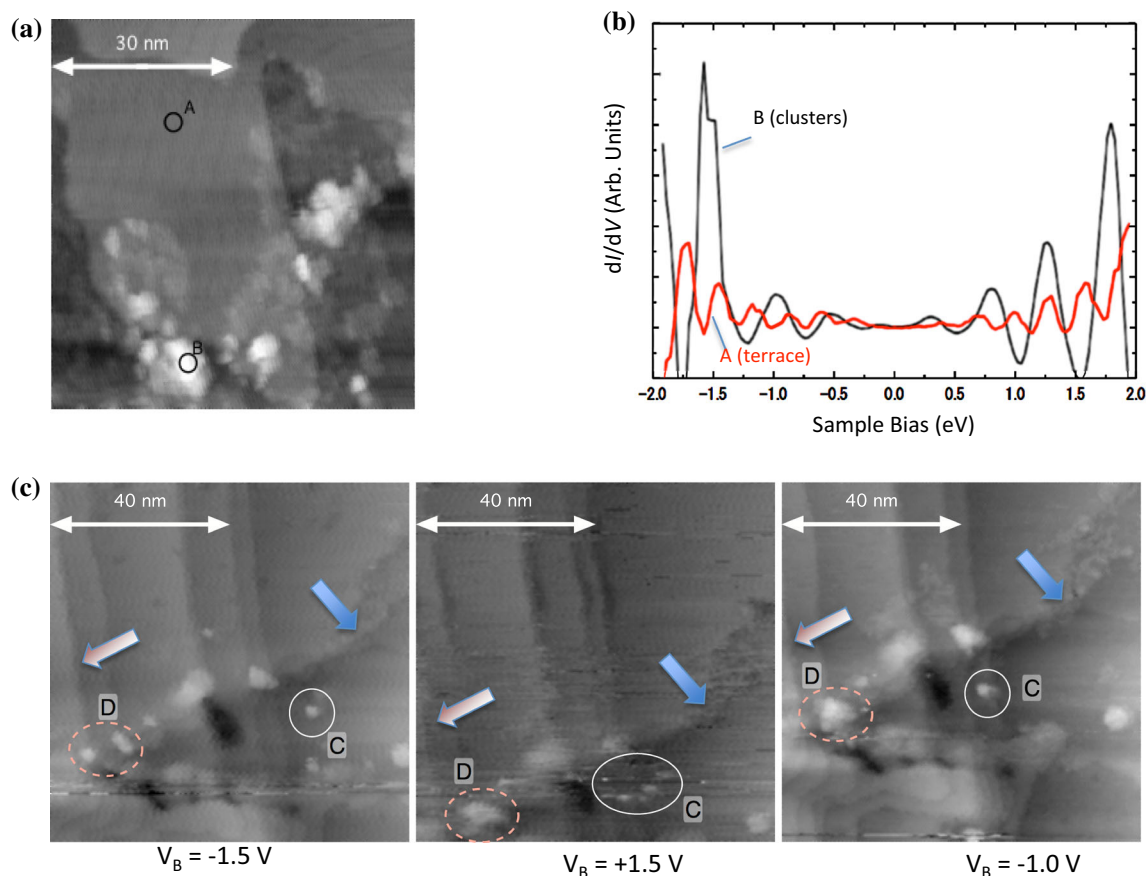

Figure 3 a STM image of an Au(111) surface after exposure to *p*CT at 0.01 L. The area shown in the image measures 60 nm × 60 nm, and the sample bias and tunneling current are 1.0 V and 0.4 nA, respectively. b STS spectra acquired at point A on the terrace of the Au(111) surface and the *p*CT cluster (point B) in image a. c STM images of *p*CT clusters formed near steps after 0.01 L exposure upon varying the sample bias voltage. The arrows are guides for the eye indicating the locations of specific steps on the surface.

Specifically, there is a peak at approximately -1.5 eV, and some oscillatory peaks above approximately $+0.8$ eV relative to E_F, which were ascribed to states of the adsorbed pCT.

As shown by the STM images presented in Fig. 3c, changing the sample bias-induced movement of the adsorbed pCT clusters. The leftmost image was acquired at a bias potential of -1.5 eV and highlights two groups of clusters, one located on a terrace (labeled C and enclosed in a white circle) and one at a step edge (labeled D and enclosed in a red dashed ellipse). Raising the bias to $+1.5$ V caused both clusters to move: cluster C separated into smaller groups, while the two clusters in D fused. Upon setting a negative bias (-1.0 eV), the scattered C cluster reassembled and occupied a position at the step edge of the higher terrace. The larger D cluster also moved and its height increased slightly, suggesting that it had merged with some neighboring molecules.

Size-dependent local spectroscopic features (STS)

Increasing the pCT exposure to ~ 0.1 L generated scattered clusters of varying size, as shown in Fig. 4a. The right-hand image is an expansion of the highlighted area of the left-hand one. Three protrusions of different sizes (labeled A, B and C) were examined; the corresponding line profiles are shown in panel (b). Protrusion A is approximately 0.5 nm tall and 0.7 nm wide. Since a pCT molecule is ~ 0.5 nm long (see Fig. 1), this protrusion consists of a single pCT molecule anchored to Au(111). Conversely, protrusion B extends over approximately 6 nm in the lateral direction and is around 0.6 nm high; it thus appears to consist of a monolayer of around 10 pCT molecules. Finally, protrusion C extends over around 10 nm laterally and is around 1.5 nm high; it thus appears to be a bilayer or trilayer comprising > 15 pCT molecules in the lateral direction. The STS spectra for the three protrusions are shown in Fig. 4c. Each curve has two strong peaks at approximately -1.2 to -1.5 and $+1.2$ to $+1.4$ eV (shadowed), which we assign to the HOMO and LUMO of the molecular adsorption states. As the cluster size increases, both peaks shift to a higher energy. However, the gap between them remains approximately 2.3 eV.

Photoemission spectroscopy (UPS)

Figure 5 shows UPS spectra of clean and pCT-adsorbed Au(111) surfaces, with binding energies calculated relative to E_F. A slight increase in intensity around -1.4 eV is discernible, but there are no apparent peaks near E_F. The intensity of the molecular adsorption peaks increased in parallel with the exposure. Adsorption had little discernible effect on the energies of the two strong peaks associated with the Au d-band at -4.5 and -6.1 eV, but increasing the exposure level increased the baseline intensity of the spectra. Adsorption of pCT caused the weak Au component at -3.9 eV to disappear and resulted in the emergence of new peaks at -2.6, -3.4 and -5.1 eV (indicated by vertical red lines). Adsorption also caused an increase in intensity without discernible peaks in the lower energy region (< -7 eV).

Discussion

If gaseous thiol molecules attack metal surfaces via the mechanism that occurs in liquid solutions [22], the resulting structure would typically be a well-ordered SAM, because a superlattice with a regular 5×5 and/or $\sqrt{19} \times \sqrt{19}$ pattern emerges as a result of Au–S bond formation via the process shown in Eq. 1 when Au(111) is immersed in an ethanolic solution of carboranethiol [20]. However, exposing Au(111) surfaces to gaseous carboranethiol did not lead to the formation of any regular pattern, as shown in Figs. 3 and 4. This discrepancy indicates that the pCT molecules diffuse and cluster on the surface because of weak intermolecular interactions. In the thiol's absence, the electron deficiency of the hydride-covered carborane surface prevents the formation of covalent bonds with metal surfaces. Therefore, until an Au–S bond happens to form, pCT simply migrates over the surface because van der Waals (vdW) attraction binds the B–C carborane shell to the surface with an energy of ~ 0.2 eV [20]. This is why even small amounts of thermal energy can induce carborane nano-wheels to migrate over metal surfaces [32]. Au–S bond formation immobilizes pCT on the gold surface until a finite energy of ~ 1 eV is applied by electron injection (Fig. 3c). This process is similar to the hopping of methylthiolate [33] induced by electron tunneling. However, it is difficult to say whether the hopping observed in our case is due to direct

Figure 4 **a** STM images of multiple differently sized *p*CT clusters on Au(111) formed at an exposure of 0.1 L. The right-hand image shows an expansion of the highlighted 58 nm × 58 nm area of the left-hand image. The sample bias and the tunneling current were 2.0 V and 0.4 nA. The image in the left was processed to facilitate recognition of steps. **b** Height profiles of clusters A, B and C along the lines shown in image **a**. **c** STS spectra for clusters A, B and C.
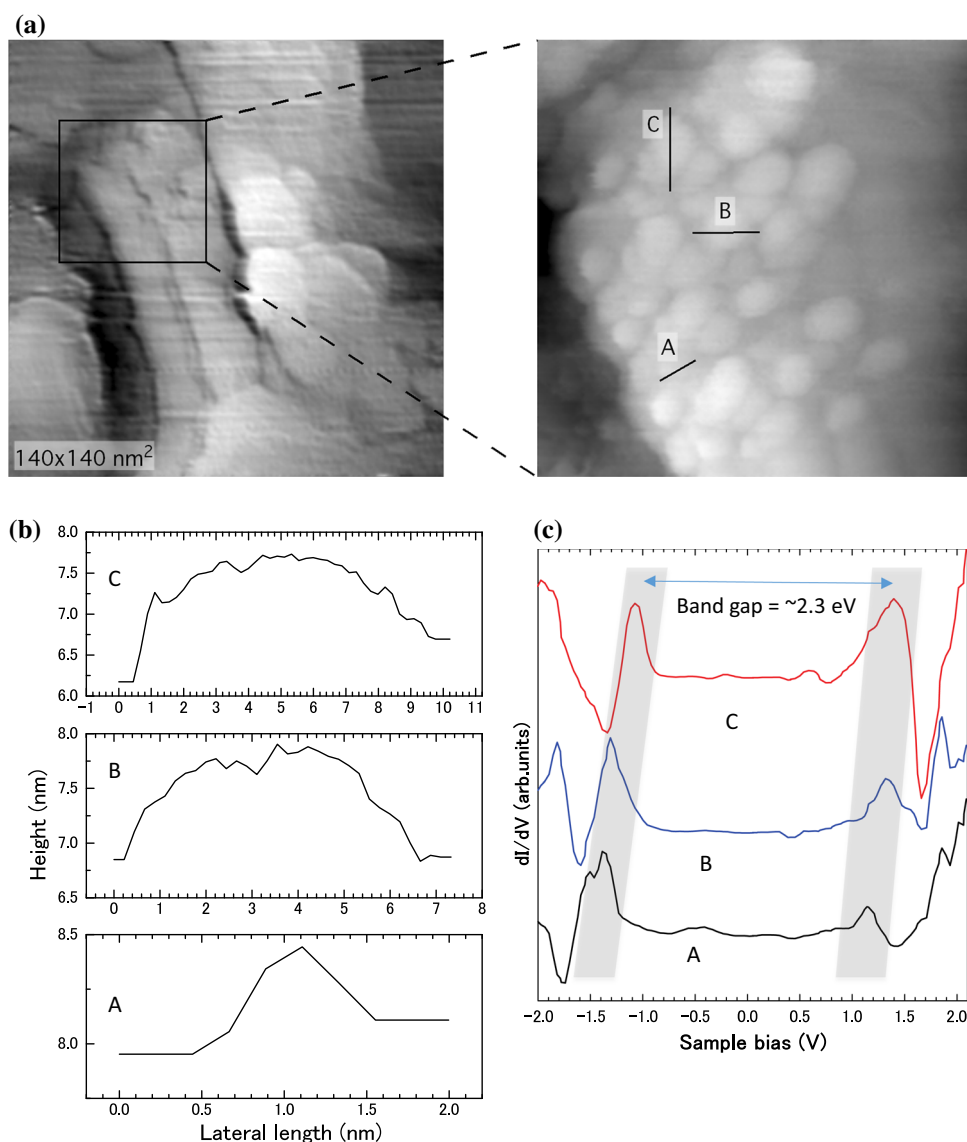
injection into unoccupied (antibonding) states at + 0.8 eV or above or excitation of the Au–S stretch due to electronic scattering at the molecular junction [33, 34].

STM images showed that *p*CT molecules formed clusters on Au(111) terraces, preferentially at step edges, during the initial stage of adsorption. The highest occupied state of *p*CT bonded to Au(111) was located at − 1.4 eV relative to E_F; this state was clearly observed by STS but not by UPS. The HOMO energy is very difficult to determine by photoemission spectroscopy [21] because the number of electrons in the HOMO is far lower than the number of electrons originating from B and C. We therefore performed theoretical calculations to clarify the

experimental results. We *first* modeled an isolated *p*CT molecule, for which three typical electronic states are shown in Fig. 6a. The large lobes at the S atom constitute the HOMO (α), while HOMO-1/HOMO-2 is conjugated π-states within the spherical B–C shell (β). Deeper states (γ, for example) are typically distributed over the molecule. Eigenvalues below E_F are indicated by × symbols in Fig. 5, in which the eigenvalues are adjusted to match the experimental HOMO peak in the STS as well as several peaks in UPS spectra. *Secondly*, we modeled the adsorbed system by placing dehydrogenated *p*CT radical(s) over a 4 × 4 Au slab. DOSs were computed for *p*CT adsorbed on Au(111) surfaces at surface coverages of 1/4 ML (one molecule per 4 × 4 slab)
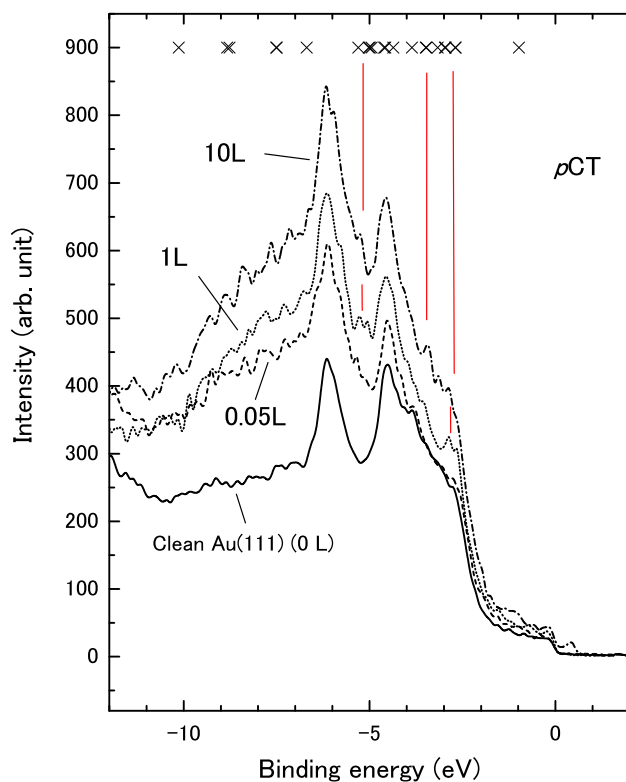
Figure 5 UPS spectra of *p*CT-adsorbed Au (111) at different exposure levels. The × symbols indicate the computationally determined energies of molecular orbitals (eigenvalues) of the isolated *p*CT molecule.

Figure 6 **a** Selected molecular orbitals of free *p*CT. **b** Calculated spectra of molecular *p*CT and molecular components of adsorbed systems.

and 1 ML (four molecules per 4 × 4 slab), as shown in Fig. 7a. Figure 6b shows partial DOSs projected onto carborane atoms from electronic states of the most stable structure of the complete adsorbed system (see the next paragraph). In this figure, the DOS of the free *p*CT molecule is shifted to fit its peaks to those of the projected DOSs. This is consistent with the approach used to fit the experimental data in Fig. 5.

To clarify the process of Au–S bond formation, three positionings of the *p*CT unit were considered: one with the S center directly above an Au atom, one with the S center bridging two adjacent Au atoms, and one with the S center above the hollow site at the center of three Au atoms; the latter proved to be the most stable after optimization in the 1/4 ML case (Fig. 7b). The C–C axis of the 1,12-carborane unit was slightly inclined (by 5.3°) from the normal of the Au(111) surface (Fig. 1c). Partial DOSs showing the components projected onto the B, C and S atoms are plotted in Fig. 8, along with the projections onto the *p*CT unit as a whole. The same procedure was
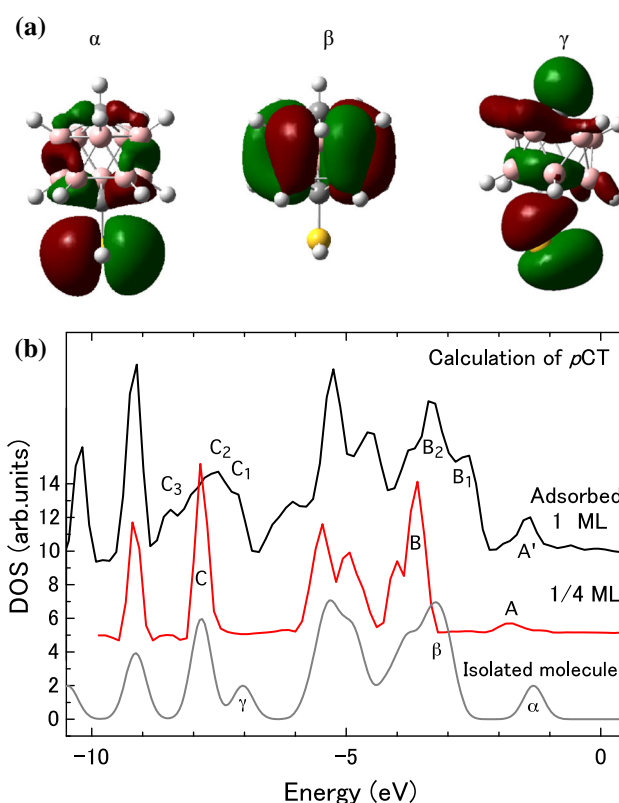

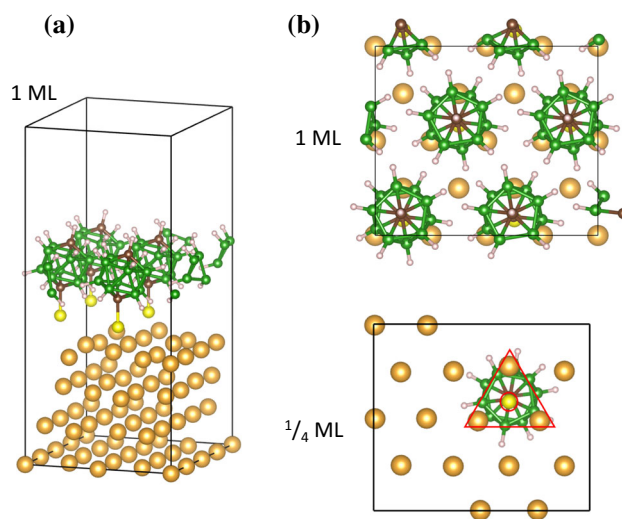**Figure 7** **a** Structure of a *p*CT-adsorbed Au(111) surface at 1 ML coverage, after optimization. **b** Bottom views of carborane molecules adsorbed on Au(111) at two different coverage levels. Both structures were obtained by geometry optimization.

followed for the 1 ML case (Figs. 6, 8). Each of the four units was most stable when placed over a hollow

site, as in the 1/4 ML case, but the C–C axis was inclined at a higher angle relative to the Au surface normal in the 1 ML case. The electron densities for selected states are shown in Fig. 8b. The B and C components, which lie between -2 and -7 eV, represent aromatic conjugated states whose energies are scarcely affected by adsorption even though the substrate has many electrons in this energy range.

The relationships between the states are illustrated in Fig. 9. The A/A' state at -1.4 eV observed by STS is shown to have a strongly localized component on S in Fig. 8a. This state is chiefly distributed over Au and S and extends into the first few layers of the gold surface. As such, it is an Au–S bonding state derived from the molecular HOMO (α). The inclination of the 1 ML case suggests that the S state retains its original p-character perpendicular to the C–S axis despite the strong intermolecular interaction with the Au(111) surface. The A′ state formed in the 1 ML case is less stable than the corresponding A state in the 1/4 ML case and is largely localized to the S center and the topmost Au layer because steric interactions between adjacent carborane units in the higher coverage 1 ML case weaken the Au–S bond. On the other hand, the resonance with the underlying Au atoms retains some of the character of the original Au surface states at -0.5 eV. This is why squeezed adsorption of carborane derivatives, as occurs during SAM formation, keeps molecular states intact. There is some evidence of this in the STS data for the single molecule case. It should be noted that the carborane shell acts as a tunneling junction, allowing the penetration of electrons. This is observable in the STS spectra, although the charge of this state is distributed in the interface region.

We next considered the second and third highest molecular states (HOMO-1 and HOMO-2; labeled β). These are almost completely degenerate, with very similar wavefunction shapes. While the electronic charge of these states is distributed inside the spherical shell, they are localized between B–H units and rather conjugated with the states of the gold substrate (state B). When multiple pCT units are placed in close proximity (as in the 1 ML case), the degeneracy of these states is broken into such as B_1 and B_2 because the structure's inclination disrupts its symmetry. This explains the broadening of the components between -2.6 and -5.1 eV in the UPS spectra. The overlap between the B–H states and the Au substrate made it almost impossible to distinguish individual degenerate electronic states in the experimental data. Because the escape length of its electrons is roughly equal to the vertical thickness of the pCT molecule, the conjugated state of the substrate generated a strong signal in the UPS spectra. The propagation of wavefunctions from a metal substrate through surface-adsorbed superaromatic molecules (C_{60}) has been reported previously [35].

Finally, we examined the electronic states of B–C bonds in the spherical shell (originating from the γ molecular state). These states lay in the region between -5 and -20 eV [21]. The spectral peaks are not sharp in this region; many of its states are distributed at high density, making it difficult to distinguish between them. Furthermore, each state's energy is very sensitive to the molecules' orientation because the electric dipole of the adsorbed carborane unit is large [23], as is often the case for aromatic materials on metal surfaces [36, 37]. These states are weakly coupled with the Au states in the first layer (states C and C_1 through C_3 in Fig. 8b), but this does not appear to affect their shapes, which closely resemble that of the molecular γ state. These states are widely distributed and should peak at approximately -7 eV according to the calculations (Fig. 6b). It is unclear why the γ state is merged into C at the low coverage. Because of the reduction of symmetry induced by further pCT adsorption, the C state in the 1/4 ML case splits into three states (C_1, C_2 and C_3) in the 1 ML case.

Summary

The structures and the electronic states of p-carboranethiol (pCT) molecules adsorbed on clean Au(111) surfaces were studied using STM/STS and UPS, revealing that adsorbed pCT molecules readily form clusters. Prior to Au–S bond formation, the molecules diffused readily over the surface even at room temperature. First principles calculations suggested that after Au–S bond formation, the HOMO of pCT and HOMO-1/HOMO-2 hybridize, forming resonant states with electrons from the topmost few layers of the substrate. We also found that a conjugated surface electronic state propagated through the pCT molecules into the vacuum above. The resonance also induced the dissolution of B–C bonds into the B–H state. Intermolecular interactions between pCT molecules adsorbed in close proximity on the

Figure 8 a Density of states of electrons projected onto the atoms of surface-adsorbed pCT units. b Spatial charge distributions of typical electronic states. States A through C_3 are designated in the same way as in Fig. 6b.
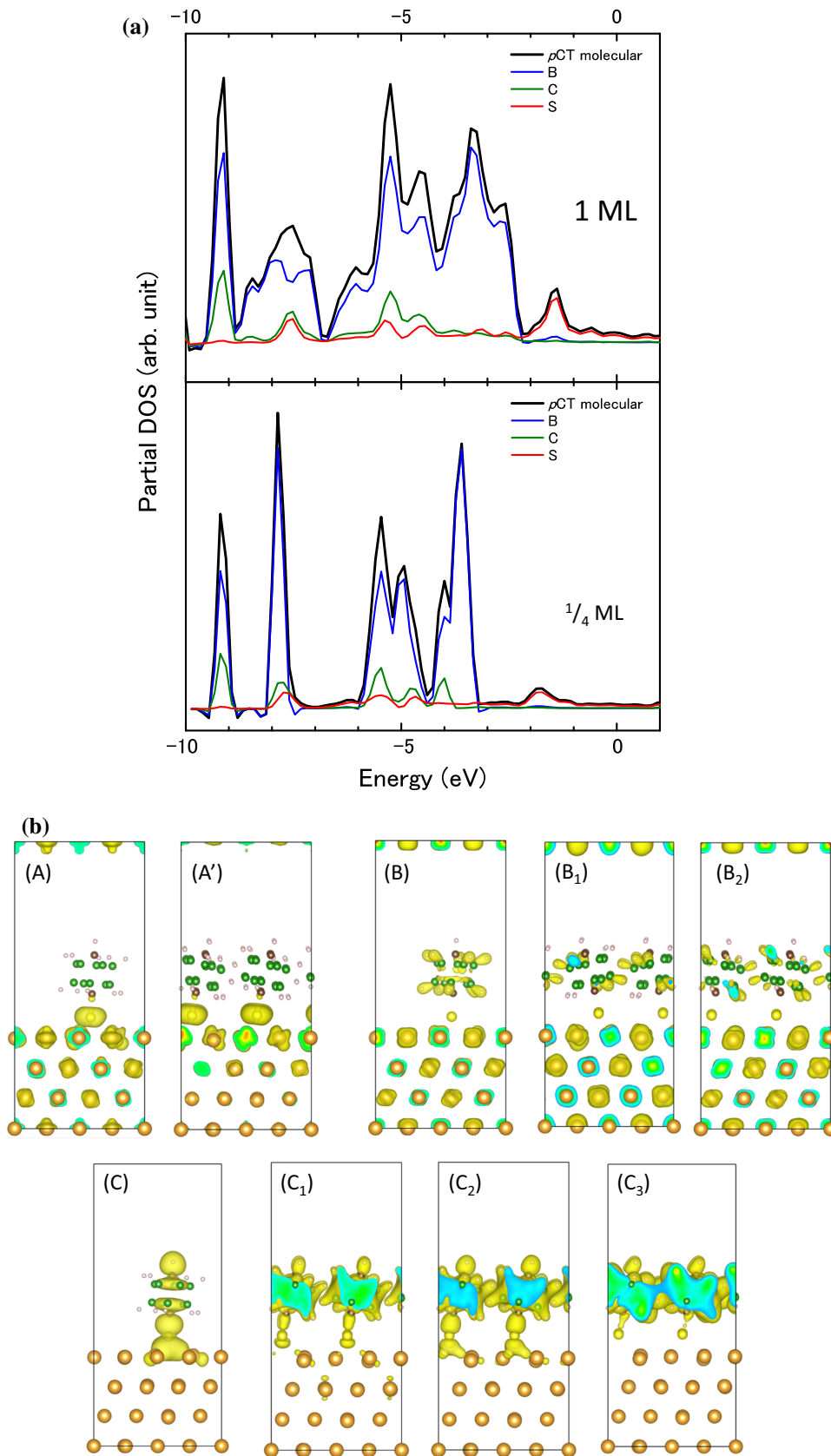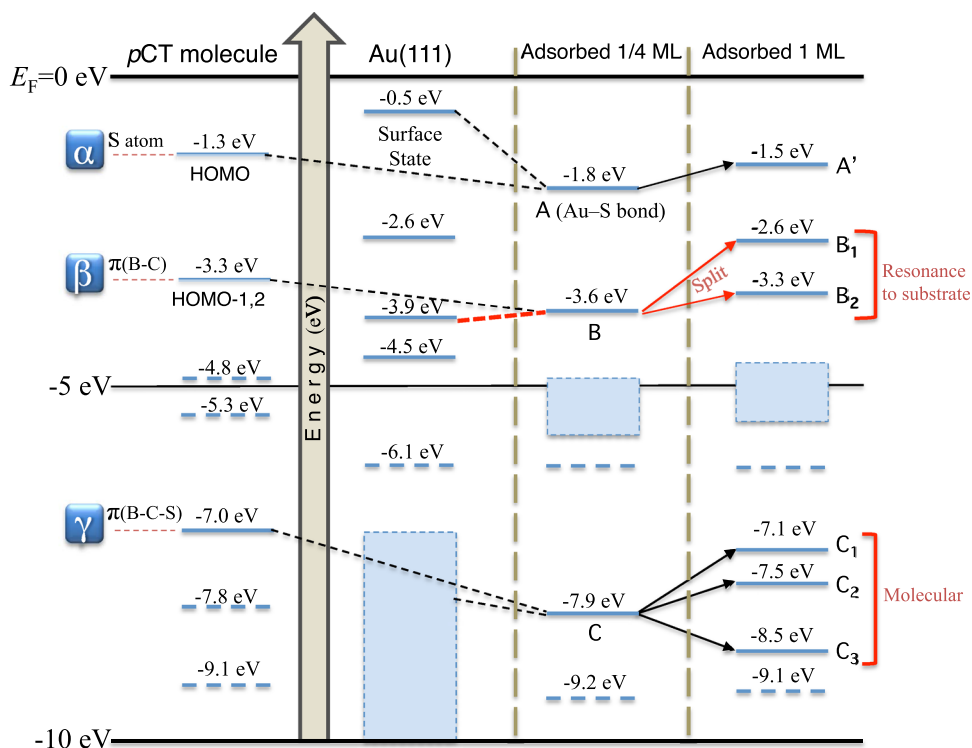
Figure 9 Energy diagram showing the relationships between the electronic states of the isolated *p*CT molecule, the Au(111) surface, and the adsorbed 1/4 ML and 1 ML systems.

substrate were mediated by substrate electrons, increasing the energy of the Au–S bond approximately at $E_F - 1.5$ eV without altering the HOMO/LUMO gap. When the density of adsorbed *p*CT was high, the adsorbate was slightly inclined relative to the surface normal, breaking the degeneracy of some states.

Overall, the results presented here indicate that vapor deposition of *p*CT under UHV results in the formation of clusters whose structures differ from those of the SAMs formed from liquid solutions. The intermolecular interactions between *p*CT and the Au surface were studied by varying the density of adsorbed molecules, and the electronic characteristics of the superaromatic molecules on the metal surface were investigated. The reported findings may facilitate the rational design of new carborane-modified surfaces with tailored properties.

Acknowledgements

References

[1] Di CA, Zhang FJ, Zhu DB (2013) Multi-functional integration of organic field-effect transistors (OFETs): advances and perspectives. Adv Mater 25:313–330

[2] Kroto HW, Heath JR, O'Brien SC, Curl RF, Smalley RE (1985) C_{60}: buckminsterfullerene. Nature 318:162–163

[3] Reed CA (2005) Carborane acids. New "strong yet gentle" acids for organic and inorganic chemistry. Chem Commun 36:1669–1677

[4] Tan C, James R, Dong B, Driver MS, Kelber JA, Downing G, Cao LR (2015) Characterization of a boron carbide-based polymer neutron sensor. Nucl Instrum Methods Phys Res A803:82–88

[5] Pasquale FL, Li Y, Du J, Kelber JA (2013) Novel alloy polymers formed from *ortho*-carborane and benzene or pyridine. J Phys Condens Matter 25:105801–105808

[6] Patel M, Swain AC, Cunningham JL, Maxwell RS, Chinn SC (2006) The stability of poly(*m*-carborane-siloxane) elastomers exposed to heat and gamma radiation. Polym Degrad Stab 91:548–554

[7] Perkinsa FK, Rosenberg RA, Lee S, Dowben PA (1991) Synchrotron-radiation-induced deposition of boron and boron carbide films from boranes and carboranes: decaborane. J Appl Phys 69:4103–4109

[8] McIlroy DN, Zhang J, Dowben PA, Heskett D (1996) Band gaps of doped and undoped films of molecular icosahedra. Mater Sci Eng A 217(218):64–68

[9] Caruso AN, Bernard L, Xu B, Dowben PA (2003) Comparison of adsorbed orthocarborane and metacarborane on metal surfaces. J Phys Chem B 107:9620–9623

[10] Januszko A, Glab KL, Kaszynski P, Patel K, Lewis RA, Mehl GH, Wand MD (2006) The effect of carborane, bicyclo[2.2.2]octane and benzene on mesogenic and dielectric properties of laterally fluorinated three-ring mesogens. J Mater Chem 16:3183–3192

[11] Schwartz JJ, Mendoza AM, Wattanatorn N, Zhao Y, Nguyen VT, Spokoyny AM, Mirkin CA, Baše T, Weiss PS (2016) Surface dipole control of liquid crystal alignment. J Am Chem Soc 138:5957–5967

[12] Grzelczak MP, Danks SP, Klipp RC, Belic D, Zaulet A, Kunstmann-Olsen C, Bradley DF, Tsukuda T, Viñas C, Teixidor F, Abramson JJ, Brust M (2017) Ion transport across biological membranes by carborane-capped gold nanoparticles. ACS Nano 11:12492–12499

[13] Huang R, Liu K, Liu H, Wang G, Liu T, Miao R, Peng H, Fang Y (2018) Film-based fluorescent sensor for monitoring ethanol–water-mixture composition via vapor sampling. Anal Chem 90:14088–14093

[14] Ni H, Qiu Z, Xie Z (2017) Photoarylation of iodocarboranes with unactivated (hetero)arenes: facile synthesis of 1,2-[(hetero)aryl]*n-o*-carboranes (*n* = 1,2) and *o*-carborane-fused cyclics. Angew Chem Int Ed 56:712–716

[15] Otsuka M, Takita R, Kanazawa T, Miyamoto K, Muranaka A, Uchiyama M (2015) Conjugation between σ- and π-aromaticity in 1-*C*-arylated monocarba-*closo*-dodecaborate anions. J Am Chem Soc 137:15082–15085

[16] Baše T, Bastl Z, Plzák Z, Grygar T, Plešek J, Carr MJ, Malina V, Šubrt J, Boháček J, Večerníková E, Kříž O (2005) Carboranethiol-modified gold surfaces. A study and comparison of modified cluster and flat surfaces. Langmuir 21:7776–7785

[17] Thomas JC, Boldog I, Auluck HS, Bereciartua PJ, Dušek M, Macháček J, Bastl Z, Weiss PS, Baše T (2015) Self-assembled *p*-carborane analogue of *p*-mercaptobenzoic acid on Au{111}. Chem Mater 27:5425–5435

[18] Ito M, Wei TX, Chen PL, Akiyama H, Matsumoto M, Tamadab K, Yamamoto Y (2005) A novel method for creation of free volume in a one-component self-assembled monolayer: dramatic size effect of *para*-carborane. J Mater Chem 15:478–483

[19] Kang J, Rowntree PA (2007) Gold film surface preparation for self-assembled monolayer studies. Langmuir 23:509–516

[20] Hohman JN, Zhang P, Morin EI, Han P, Kim M, Kurland AR, McClanahan PD, Balema VP, Weiss PS (2009) Self-assembly of carboranethiol isomers on Au{111}: intermolecular interactions determined by molecular dipole orientations. ACS Nano 3:527–536

[21] Scholz F, Nothofer HG, Wessels JM, Nelles G, Wrochem FV, Roy S, Chen X, Michl J (2011) Permethylated 12-vertex *p*-carborane self-assembled monolayers. J Phys Chem C 115:22998–23007

[22] Ulman A (1996) Formation and structure of self-assembled monolayers. Chem Rev 96:1533–1554

[23] Balaz S, Caruso AN, Platt NP, Dimov DI, Boag NM, Brand JI, Losovyj YB, Dowben PA (2007) The influence of the molecular dipole on the electronic structure of isomeric icosahedral dicarbadodecaborane and phosphacarbadodecaborane molecular films. J Phys Chem B 111:7009–7016

[24] Wrochem FV, Scholz F, Gao D, Nothofer HG, Yasuda A, Wessels JM, Roy S, Chen X, Michl J (2010) High-band-gap polycrystalline monolayers of a 12-vertex *p*-carborane on Au(111). J Phys Chem Lett 1:3471–3477

[25] Plešek J, Heřmánek S (1981) Syntheses and properties of substituted icosahedral carborane thiols. Collect Czech Chem Commun 46:687–692

[26] Barth JV, Brune H, Ertl G, Behm RJ (1990) Scanning tunneling microscopy observations on the reconstructed Au(111) surface: atomic structure, long-range superstructure, rotational domains, and surface defects. Phys Rev B 42:9307–9318

[27] Narasimhan S, Vanderbilt D (1992) Elastic stress domains and the herringbone reconstruction on Au(111). Phys Rev Lett 69:1564–1567

[28] Kevan SD, Gaylord RH (1987) High-resolution photoemission study of the electronic structure of the noble-metal (111) surfaces. Phys Rev B 36:5809–5818

[29] Avouris P, Lyo IW, Walkup RE, Hasegawa Y (1994) Real space imaging of electron scattering phenomena at metal surfaces. J Vac Soc Technol B 12:1447–1455

[30] http://www.gaussian.com/. Accessed 9 Apr 2019

[31] https://www.vasp.at/. Accessed 9 Apr 2019

[32] Shirai Y, Morin JF, Sasaki T, Guerreroa JM, Tour JM (2006) Recent progress on nanovehicles. Chem Soc Rev 35:1043–1055

[33] Ohara M, Kim Y, Kawai M (2006) Tunneling-electron-induced hopping of methylthiolate on Cu(111). Jpn J Appl Phys 45:2022–2025

[34] Momose T, Shudo K, Raebiger H, Ohno S, Kitajima T, Uchiyama M, Suzuki T, Tanaka M (2014) Molecular motion induced by multivibronic excitation on semiconductor surface. J Phys Chem C 118:1554–1559

[35] Aoki M, Kamada T, Sasaki K, Masuda S, Morikawa Y (2012) Chemisorption-induced gap states at organic–metal interfaces: benzenethiol and benzeneselenol on metal surfaces. Phys Chem Chem Phys 14:4101–4108

[36] Britton AJ, Rienzo A, O'Shea JN, Schulte K (2010) Charge transfer between the Au(111) surface and adsorbed C_{60}: resonant photoemission and new core-hole decay channels. J Chem Phys 133:094705

[37] Yun DJ, Shin WH, Bulliard X, Park JH, Kim S, Chung JG, Kim Y, Heo S, Kim SH (2016) Direct characterization of the energy level alignments and molecular components in an organic hetero-junction by integrated photoemission spectroscopy and reflection electron energy loss spectroscopy analysis. Nanotechnology 27:345704–345714